Applied Physics Express

LETTERS

Multispectral selective near-perfect light absorption by graphene monolayer using aperiodic multilayer microstructures

Applied Physics Express **11**, 035101 (2018)
https://doi.org/**10.7567/APEX.11.035101**

Multispectral selective near-perfect light absorption by graphene monolayer using aperiodic multilayer microstructures

Iman Zand[1,2,6*], Hamed Dalir[3*], Ray T. Chen[4], and Jonathan P. Dowling[1,2,5]

[1]*Center for Computation and Technology, Louisiana State University, Baton Rouge, LA 70803, U.S.A.*
[2]*Hearne Institute of Theoretical Physics and Department of Physics and Astronomy, Louisiana State University, Baton Rouge, LA 70803, U.S.A.*
[3]*Omega Optics, Inc., Austin, TX 78757, U.S.A.*
[4]*Department of Electrical and Computer Engineering, University of Texas at Austin, Austin, TX 78758, U.S.A.*
[5]*New York University Shanghai, Shanghai 200122, China*
[6]*Hub Petroleum, New Orleans, LA 70163, U.S.A.*

*E-mail: izand@hubpetroleum.com; hamed.dalir@omegaoptics.com

Received January 17, 2018; accepted February 6, 2018; published online February 23, 2018

We investigate one-dimensional aperiodic multilayer microstructures in order to achieve near-total absorptions at preselected wavelengths in a graphene monolayer. The proposed structures are designed using a genetic optimization algorithm coupled to a transfer matrix code. Coupled-mode-theory analysis, consistent with transfer matrix method results, indicates the existence of a critical coupling in the graphene monolayer for perfect absorptions. Our findings show that the near-total-absorption peaks are highly tunable and can be controlled simultaneously or independently in a wide range of wavelengths in the near-infrared and visible ranges. The proposed approach is metal-free, does not require surface texturing or patterning, and can be also applied for other two-dimensional materials.

Graphene, a one-atom-thick two-dimensional (2D) material, has opened a new horizon for researchers owing to its unique electronic and optical properties.[1–5] However, one of the critical issues in the design of graphene-based optical devices is the enhancement of light absorption in order to achieve a near-total absorption. In the mid- to far-infrared range, various optical structures based on patterned graphene[6,7] and unpatterned graphene[8–10] have been introduced. These structures utilize the plasmonic response of graphene. On the other hand, in the visible and near-infrared regimes, undoped unpatterned graphene does not exhibit a plasmonic response;[11] it absorbs only approximately 2.3% of the light at normal incidence.[12] In order to enhance light absorption in graphene monolayer, plasmonic antennas,[13] photonic crystal slabs,[14–17] and Fabry–Perot microcavities[18–27] have been studied.

Among the proposed platforms, one-dimensional (1D) dielectric multilayers are promising candidates owing to their simple design and low amount of optical loss compared with metallic structures. In previous studies based on 1D multilayer structures, localization of light near a graphene monolayer has been achieved by placing graphene inside an asymmetric Fabry–Perot cavity, with a partially reflective front mirror and perfect back mirror. As in the visible and near-infrared regimes undoped graphene does not exhibit plasmonic response, the coupling of light to graphene is governed by the properties of resonance modes of the 1D multilayer structures. Therefore, the spatial localization of longitudinal resonant modes of the multilayer structure directly influences the absorption spectrum of the graphene monolayer. One of the efficient approaches to control the spatial localization of resonance modes in 1D structures is to use aperiodic multilayers supporting asymmetric/symmetric and extended/localized field profiles.[28,31] Compared with asymmetric-Fabry–Perot-based designs, aperiodic structures provide more degrees of freedom and efficiency for the spatial selective localization of the resonant modes. Although in asymmetric Fabry–Perot designs, the front and back mirrors are composed of periodic layers, in aperiodic multilayers both sides of the graphene monolayer are non-periodic multilayers with arbitrary layers' thicknesses.

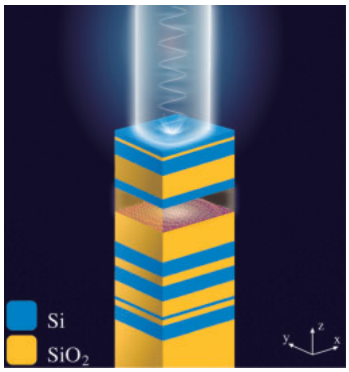

Fig. 1. Schematic of the 1D aperiodic multilayer composed of alternating layers of silicon (blue) and silica (yellow) on top of a semi-infinite silicon substrate. The graphene monolayer (red) is placed inside the structure.

Therefore, owing to the importance for applications requiring multispectral light detection, in this study, aperiodic multilayers are proposed as efficient platforms to enhance (~100% absorption) and tune the light absorption in graphene monolayer at multiple preselected wavelengths. We optimize the thicknesses using a genetic optimization algorithm,[29–31] coupled to a transfer matrix code, in order to maximize the absorption of the graphene monolayer at desired preselected wavelengths. In addition, coupled-mode theory (CMT) is employed to explain the physical mechanisms of the resonating structures. Our simulation results show that the proposed approach not only provides a near-total light absorption at preselected multiple wavelengths but it also enables to efficiently tune these wavelengths either simultaneously or independently.

A schematic of the aperiodic design is shown in Fig. 1. A graphene monolayer is placed inside a 1D aperiodic multilayer composed of alternating layers of silicon and silica deposited on a silica substrate. The two adjacent layers of the graphene monolayer are set to be SiO_2 in order to provide a homogeneous environment surrounding the graphene monolayer. We model the optical properties of silicon and silica based on the experimental data in Ref. 32, while the graphene monolayer is characterized as in Refs. 14 and 15. The first layer of

the top (bottom) multilayer is silicon (silica), while the last layer is silica (silicon). For simplicity, we refer to the structures as M_iN_j, where M and N denote the top and bottom multilayers, respectively, while i and j are the numbers of layers. The top multilayer consists of 6 layers, while the bottom multilayer consists of 16 or 18 layers. The thicknesses of all layers are allowed to vary between 40 and 600 nm. In our simulations, the light is incident from the air into the structures.

Our main aim is to design 1D aperiodic multilayers with a highly tunable near-total absorption by the graphene monolayer at preselected wavelengths. We employ a hybrid optimization algorithm in combination with the transfer matrix method (TMM) to maximize the absorption in the graphene monolayer at multiple preselected wavelengths. The optimization algorithm consists of a microgenetic global optimization algorithm coupled to an optimization suite packaged by the Massachusetts Institute of Technology, called NLOPT.[29–31] This algorithm enables to determine the best structures' dimensions for a varying number of layers at a given wavelength λ_i. In order to maximize the absorption at several wavelengths, we maximize the fitness function, $F = \sum_{i=1}^{n} A(\lambda_i)$, where $A(\lambda_i)$ is the absorption in the graphene monolayer at a wavelength of λ_i.

In order to calculate the optical power absorbed in the graphene monolayer, we calculate the total reflection (R) of the aperiodic structure to obtain the field amplitude of the reflected wave. The field amplitudes in the adjacent layers of the graphene monolayer can be determined by matrix multiplication of the individual components of the layers, starting from the first region (which is air) and proceeding to the adjacent layers. Once the forward and backward fields in the vicinity of the graphene monolayer are determined, their corresponding Poynting vectors can be employed to compute the optical power absorbed by the graphene monolayer:[19]

$$A(\lambda, \theta) = S_{\text{in}}(\lambda, \theta) - S_{\text{out}}(\lambda, \theta), \tag{1}$$

where A is the absorbance, S_{in} (S_{out}) is the optical power entering (leaving) the graphene monolayer, λ is the wavelength, and θ is the angle between the incident light direction and z-axis (normal to the structure). As we aim to optimize the structures for normal incidence of light, θ is set to zero in the optimizations.

Using the TMM and genetic algorithm, we investigate the tunability of the 1D aperiodic multilayers for a single-wavelength light absorption. Figure 2 shows that when the structures S1, S2, and S3 are optimized for preselected absorption wavelengths, a near-total resonant light absorption by the graphene monolayer is observed. The absorption wavelengths are set to 1.2 μm (black curve), 1.55 μm (green curve), and 1.9 μm (blue curve); the M_6N_{12} structure is employed. Any desired wavelengths from the spectrum window can be selected, and the genetic optimization provides proper aperiodic multilayers to ensure 100% light absorption. It should be mentioned that various aperiodic structures correspond to a specific selected wavelength; we presented only one of them for each case.

The normalized E-field amplitude profiles, shown as insets in Fig. 2, indicate resonant enhancements of the E-fields at the graphene surface for all three absorption wavelengths, which lead to an almost 100% light absorption in the

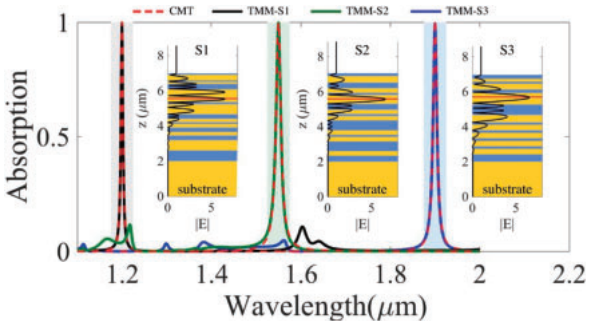

Fig. 2. Absorption spectra of three genetic-algorithm-optimized M_6N_{12} structures (S1, S2, and S3) for single-wavelength absorptions at 1.2 μm (black curve), 1.55 μm (green curve), and 1.9 μm (blue curve). The results are compared with those obtained using CMT (dashed red curve), which demonstrates an excellent agreement near resonances. The CMT curves are disconnected; they were calculated individually for each peak. The corresponding E-field profiles of the absorption, shown as insets, illustrate the strong enhancement of the E-fields near the graphene monolayer. The normalized E-field amplitudes at the graphene surface, for all cases, are approximately 6.5. The blue, yellow, and red layers, represent silicon, silica, and graphene monolayer, respectively.

graphene monolayer. The E-fields at the graphene surface (E_g) are approximately equal: 6.57 (S1), 6.58 (S2), and 6.56 (S3). As graphene is an ultra-thin material, it acts as a small perturbation to the system and does not disturb the E-field profiles of the resonance modes of the original structures (without graphene). However, it decreases the enhancement factors of the structures and rescales the field profiles. For example, the maximum values of the E-fields (E_{max}) of $\{S1, S2, S3\}$ are $\{12.47, 13.15, 12.92\}$ (without graphene) and $\{6.57, 6.6, 6.56\}$ (with graphene), which shows that the enhancement factors of the structures decreased by a factor of 2. In general, the approximately equal amplitudes of the E-fields at the graphene position for different wavelengths and rescaled profiles of the absorption modes over the wide range of wavelengths stem from a relatively small change of graphene loss; this indicates the critical coupling of the incoming waves to the graphene monolayer.

An aperiodic multilayer with a graphene monolayer acts as a lossy resonating system with three possible states of under-coupling, critical coupling, and over-coupling. When the external leakage rate of the resonance mode and intrinsic loss rates are equal, a perfect absorption in the graphene monolayer occurs, and the system exhibits critical coupling. This can be explained by CMT, based on input–output properties of a resonating system and coherent interference of direct and indirect pathways.[14,33] As the designed structures exhibit an almost 100% light reflection at the selected wavelengths, in the absence of graphene, they can be modeled as a one-port resonating system. Therefore, the absorption spectrum of the graphene monolayer near the absorption wavelengths for a multi-resonance system can be described as

$$A(\omega) = \sum_{i=1}^{n} 4\delta_i\gamma_i/[(\omega - \omega_{0i})^2 + (\delta_i + \gamma_{ei})^2], \tag{2}$$

where ω_{0i} is the absorption resonance frequency, and γ_{ei} and δ_i are the external leakage rate and intrinsic loss rate at each resonance frequency, respectively. As Eq. (2) suggests, for a resonating structure with equal intrinsic loss and external leakage rates (critical coupling), the absorption is one (100%).

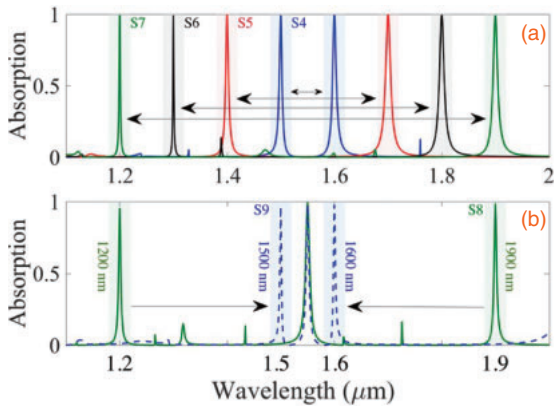

Fig. 3. Absorption spectra of the genetic-algorithm-optimized structures as a function of the wavelength at normal incidence for preselected wavelengths (μm) of (a) S4: {1.5, 1.6}, S5: {1.4, 1.7}, S6: {1.3, 1.8}, and S7: {1.2, 1.9}, and (b) S8: {1.2, 1.55, 1.9}, and S9: {1.5, 1.55, 1.6}. The preselected wavelengths are tuned simultaneously and independently. M_6N_{16} (M_6N_{18}) arrangement is employed for the double-(triple-)wavelength absorptions.

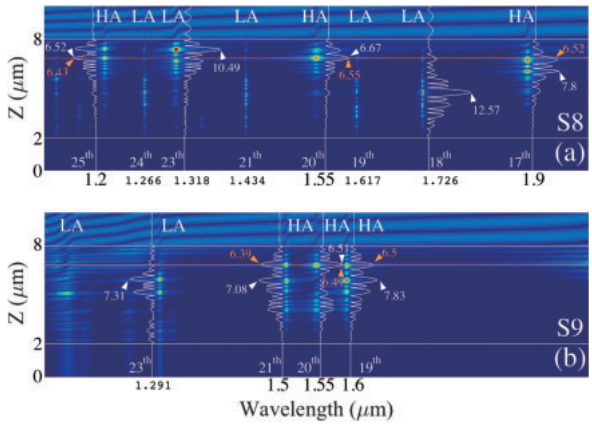

Fig. 4. Normalized *E*-field amplitudes (λ–z maps) of the S8 and S9 structures for absorption wavelength of {1.5, 1.55, 1.6} and {1.2, 1.55, 1.9}. Low-absorption resonance modes (LA-modes) are also excited in addition to the high-absorption resonance modes (HA-modes). The orange arrows indicate the E_g of the HA-modes. The modes' numbers are determined based on the number of *E*-field antinodes in the structures.

Non-equal rates lead to a partial absorption (over-coupling/under-coupling states). In order to validate this analysis, TMM simulations are compared with CMT results, which, as demonstrated in Fig. 2, show an excellent agreement.

According to the above discussion, the small variation of graphene loss and stable critical coupling to graphene in a wide range of frequencies, provide a simultaneous tuning of multi-wavelength absorptions of the graphene monolayer and similar *E*-field amplitudes at the graphene surface. In order to demonstrate this analysis, we optimize the M_6N_{16} structures to obtain perfect double-wavelength light absorptions. Figure 3(a) shows that when each structure is optimized for two preselected wavelengths of $\{\lambda_1\ (\mu m), \lambda_2\ (\mu m)\}$, a near-total resonant light absorption occurs in the graphene monolayer at these wavelengths. The absorption wavelengths are set to {1.5, 1.6} (blue curve), {1.4, 1.7} (red curve), {1.3, 1.8} (black curve), and {1.2, 1.9} (green curve). These preselected wavelengths are simultaneously tuned in a broad wavelength range extending from ∼1.2 to ∼1.9 μm. The corresponding E_g of these wavelengths (from the shortest to the longest) are 6.56, 6.46, 6.51, 6.54, 6.56, 6.58, 6.56, and 6.55, respectively.

Furthermore, we optimize M_6N_{18} multilayers to absorb optical waves at three preselected wavelengths of $\{\lambda_1\ (\mu m), \lambda_2\ (\mu m), \lambda_3\ (\mu m)\}$. In this case, one of the preselected absorption wavelengths (λ_2) is set to 1.55 μm, while the other two wavelengths (λ_1, λ_3), independently from λ_1, are simultaneously tuned from {1.2, 1.9} to {1.5, 1.6}. As shown in Fig. 3(b), a near-perfect absorption of incident light is achieved at preselected wavelengths of {1.2, 1.55, 1.9} and {1.5, 1.55, 1.6}.

In Fig. 4, we show the λ–z maps of the normalized *E*-field amplitudes for the genetic-algorithm-optimized structures S8 and S9, described in Fig. 3. The position of the graphene monolayer and structure boundaries are indicated by the orange and white lines, respectively. E_{max} and E_g are indicated by the white and orange arrows, respectively. Moreover, 1D plots of the *E*-fields of some of the resonance modes of the S8 and S9 structures are shown as insets (white). Two types of high-absorption (HA-modes: 17th, 20th, and 25th for S8 and 19th, 20th, and 21th for S9) and low-absorption (LA-modes: 17th and 22th for S8 and 23th for S9) modes coexist in the structures. These modes exhibit different E_{max} (white arrows), penetration depths, and frequency spreading. In S8, E_{max} of the 18th is considerably larger than those of the other modes, which can be attributed to the relatively symmetric distribution of the *E*-field at the center of the structure and its localization far away from the graphene monolayer. Critical coupling of the 23th mode is prohibited, and no absorption is observed, as the position of the graphene monolayer is at the node of the *E*-field profile. Similar behavior is also observed for the S9 structure. Moreover, similar to the previous cases, E_g of the HA-modes are similar and approximately equal to 6.5, which is, in general, valid for any other optimized structures with perfect (almost perfect) absorptions.

The angular aperture of the incident light lowers the maximum absorption as there is a deviation from the ideal 1D propagation. For a comparison of the structures, we define an angular FWHM, $\delta\theta$, by calculating the width around $\theta = 0$ for which the absorbance is larger than half of the maximum achieved by the genetic optimization for normal incidence. We also define a spectral FWHM $\delta\lambda$ for the aperiodic structures, by calculating the width around the absorption wavelengths (at which we optimized the structures), for which the absorption is larger than half of the maximum values at the preselected wavelengths. The results are summarized in Table I. Both transverse electric (TE) and transverse magnetic (TM) modes exhibit similar $\delta\theta$. The absorption process can be considered polarization-independent around the normal incidence. Moreover, absorptions with lower $\delta\lambda$ (higher *Q*-factors; $Q = \lambda/\delta\lambda$) exhibit smaller $\delta\theta$ and higher angular sensitivity.

Further, we investigate perfect absorptions by aperiodic structures with selectable multiple wavelengths in the visible spectrum. Considering the scalability of photonic structures, a similar behavior applies to the visible wavelengths; a difference is the need to use proper lossless optical materials. In the visible regime, the available range of index contrast is smaller than that at the near-infrared regime, and in addition, the losses in silicon become considerable. Therefore, we opti-

Table I. Angular FWHM $\delta\theta$TE/TM (deg) and spectral FWHM $\delta\lambda$ (nm) of the structures described in Fig. 3.

Double-wavelength absorptions (μm) [Fig. 3(a)]				
$\{\lambda_1, \lambda_2\}$	$\{1.2, 1.9\}$	$\{1.3, 1.8\}$	$\{1.4, 1.7\}$	$\{1.5, 1.6\}$
$\{\delta\lambda_1, \delta\lambda_2\}$	$\{2.6, 9.9\}$	$\{2.1, 10.3\}$	$\{6.2, 11.2\}$	$\{6.0, 8.1\}$
$\{\delta\theta_{TM1}, \delta\theta_{TM2}\}$	$\{10.9, 15.1\}$	$\{10.2, 16.8\}$	$\{16.9, 19.3\}$	$\{12.2, 14.7\}$
$\{\delta\theta_{TE1}, \delta\theta_{TE2}\}$	$\{10.3, 16\}$	$\{11.2, 18.0\}$	$\{16.9, 19.2\}$	$\{12.6, 14.6\}$

Triple-wavelength absorptions (μm) [Fig. 3(b)]		
$\{\lambda_1, \lambda_2, \lambda_3\}$	$\{1.2, 1.55, 1.9\}$	$\{1.5, 1.55, 1.6\}$
$\{\delta\lambda_1, \delta\lambda_2, \delta\lambda_3\}$	$\{4.5, 8.9, 5.6\}$	$\{3.4, 6.2, 4.1\}$
$\{\delta\theta_{TM1}, \delta\theta_{TM2}, \delta\theta_{TM3}\}$	$\{14.8, 17.2, 13.1\}$	$\{10.8, 15.6, 13.4\}$
$\{\delta\theta_{TE1}, \delta\theta_{TE2}, \delta\theta_{TE3}\}$	$\{15.5, 17, 14.8\}$	$\{11.2, 15.7, 12.1\}$

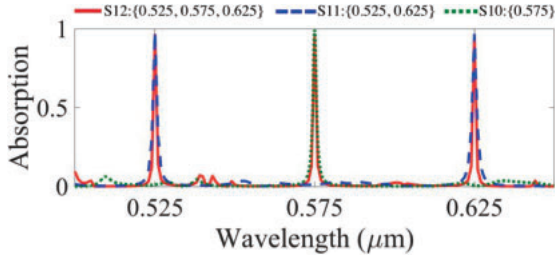

Fig. 5. Absorption spectra of the genetic-algorithm-optimized structures as a function of the wavelength at normal incidence for preselected wavelengths (μm) of S10: {0.575}, S11: {0.525, 0.625}, and S12: {0.525, 0.575, 0.625}.

mize aperiodic multilayers composed of alternating layers of tantalum pentoxide (Ta_2O_5) and silica deposited on a silica substrate for the wavelength range of 500–650 nm. Ta_2O_5, is lossless in this regime and exhibits a refractive index of ~2.12.

As shown in Fig. 5, almost perfect absorptions were achieved for preselected wavelengths (μm) of {0.575}, {0.525, 0.625}, and {0.525, 0.575, 0.625}. These wavelengths can be tuned both simultaneously and independently as discussed for the previous case. The genetic-algorithm-optimized structures for single-, double-, and triple-wavelength absorptions are $M_{14}N_{26}$, $M_{18}N_{34}$, and $M_{18}N_{34}$, respectively. In this case, the aperiodic structures exhibit a larger number of layers, compared with the near-infrared structures, owing to the low index contrast between Ta_2O_5 and SiO_2, compared with that between Si and SiO_2, whose n_H/n_L ratios are approximately 1.46 and 2.4, respectively.

In summary, we demonstrated that 1D aperiodic multilayer structures can be successfully optimized to achieve a near-total absorption in the graphene monolayer at preselected wavelengths. These absorption peaks were highly tunable and could be controlled either simultaneously or independently. Simulation results revealed that the normalized E-field at the graphene surface was always approximately 6.5 at the perfect (almost perfect) absorption. The proposed platform is a promising candidate to design multispectral light detection devices and filters; in addition, it is metal-free and does not require surface texturing or patterning. The presented concept is also applicable for other 2D materials.

Acknowledgments J.P.D. would like to acknowledge support from the Army Research Office and Defense Advanced Research Projects Agency. H.D. and R.T.C. are supported by Air Force Office of Scientific Research (AFOSR), (FA9550-17-P-0014) of the small business innovation research (SBIR) program.

1) V. W. Brar, A. R. Koltonow, and J. Huang, ACS Photonics **4**, 407 (2017).
2) R. Yu, V. Pruneri, and F. J. G. de Abajo, ACS Photonics **2**, 550 (2015).
3) A. N. Grigorenko, M. Polini, and K. S. Novoselov, Nat. Photonics **6**, 749 (2012).
4) L. Zhu, F. Liu, H. Lin, J. Hu, Z. Yu, X. Wang, and S. Fan, Light: Sci. Appl. **5**, e16052 (2016).
5) H. Dalir, Y. Xia, Y. Wang, and X. Zhang, ACS Photonics **3**, 1564 (2016).
6) J. Christensen, A. Manjavacas, S. Thongrattanasiri, F. H. L. Koppens, and F. G. J. de Abajo, ACS Nano **6**, 431 (2012).
7) S. Thongrattanasiri, F. H. L. Koppens, and F. J. García de Abajo, Phys. Rev. Lett. **108**, 047401 (2012).
8) W. Gao, J. Shu, C. Qiu, and Q. Xu, ACS Nano **6**, 7806 (2012).
9) T. R. Zhan, F. Y. Zhao, X. H. Hu, X. H. Liu, and J. Zi, Phys. Rev. B **86**, 165416 (2012).
10) X. Zhu, W. Yan, P. Uhd Jepsen, O. Hansen, N. A. Mortensen, and S. Xiao, Appl. Phys. Lett. **102**, 131101 (2013).
11) F. Xia, H. Yan, and P. Avouris, Proc. IEEE **101**, 1717 (2013).
12) R. R. Nair, P. Blake, A. N. Grigorenko, K. S. Novoselov, T. J. Booth, T. Stauber, N. M. R. Peres, and A. K. Geim, Science **320**, 1308 (2008).
13) Z. Fang, Z. Liu, Y. Wang, P. M. Ajayan, P. Nordlander, and N. J. Halas, Nano Lett. **12**, 3808 (2012).
14) J. R. Piper and S. H. Fan, ACS Photonics **1**, 347 (2014).
15) Y. Liu, A. Chadha, D. Zhao, J. R. Piper, Y. Jia, Y. Shuai, L. Menon, H. Yang, Z. Ma, S. Fan, F. Xia, and W. Zhou, Appl. Phys. Lett. **105**, 181105 (2014).
16) Y. Long, L. Shen, H. Xu, H. Deng, and Y. Li, Sci. Rep. **6**, 32312 (2016).
17) Y. S. Fan, C. C. Guo, Z. H. Zhu, W. Xu, F. Wu, X. D. Yuan, and S. Q. Qin, Opt. Express **25**, 13079 (2017).
18) M. Engel, M. Steiner, A. Lombardo, A. C. Ferrari, H. V. Lohneysen, P. Avouris, and R. Krupke, Nat. Commun. **3**, 906 (2012).
19) A. Ferreira, N. M. R. Peres, R. M. Ribeiro, and T. Stauber, Phys. Rev. B **85**, 115438 (2012).
20) J.-T. Liu, N.-H. Liu, J. Li, X. J. Li, and J.-H. Huang, Appl. Phys. Lett. **101**, 052104 (2012).
21) M. Furchi, A. Urich, A. Pospischil, G. Lilley, K. Unterrainer, H. Detz, P. Klang, A. M. Andrews, W. Schrenk, G. Strasser, and T. Mueller, Nono Lett. **12**, 2773 (2012).
22) M. A. Vincenti, D. de Ceglia, M. Grande, A. D'Orazio, and M. Scalora, Opt. Lett. **38**, 3550 (2013).
23) J. Zheng, R. A. Barton, and D. Englud, ACS Photonics **1**, 768 (2014).
24) B. Vasić and R. Gajić, Opt. Lett. **39**, 6253 (2014).
25) M. A. Vincenti, D. de Ceglia, M. Grande, A. D'Orazio, and M. Scalora, Phys. Rev. B **89**, 165139 (2014).
26) L. Jiang, J. Guo, L. Wu, X. Dai, and Y. Xiang, Opt. Express **23**, 31181 (2015).
27) Y.-B. Wu, W. Yang, T.-B. Wang, X.-H. Deng, and J.-T. Liu, Sci. Rep. **6**, 20955 (2016).
28) L. D. Negro, *Optics of Aperiodic Structures: Fundamentals and Device Applications* (Pan Stanford Publishing, Singapore, 2014).
29) K. Krishnakumar, Proc. SPIE **1196**, 289 (1990).
30) S. G. Johnson, NLOPT: Nonlinear-Optimization Package (2008).
31) C. H. Granier, F. O. Afzal, C. Min, J. P. Dowling, and G. Veronis, J. Opt. Soc. Am. B **31**, 1316 (2014).
32) D. R. Lide, *CRC Handbook of Chemistry and Physics* (CRC Press, Boca Raton, FL, 2007) 88th ed.
33) H. A. Haus, *Waves and Fields in Optoelectronics* (Prentice-Hall, Englewood Cliffs, NJ, 1984).